JOURNAL OF GEOPHYSICAL RESEARCH, VOL. 102, NO. C11, PAGES 25,035-25,046, NOVEMBER 15, 1997

Modeling spectra of breaking surface waves in shallow water

Yongze Chen and R.T. Guza

Center for Coastal Studies, Scripps Institution of Oceanography, La Jolla, California

Steve Elgar

School of Electrical Engineering and Computer Science, Washington State University, Pullman

Abstract. Predictions from Boussinesq-equation-based models for the evolution of breaking surface gravity waves in shallow water are compared with field and laboratory observations. In the majority of the 10 cases investigated, the observed spectral evolution across the surf zone is modeled more accurately by a dissipation that increases at high frequency than by a frequency-independent dissipation. However, in each case the predicted spectra are qualitatively accurate for a wide range of frequency-dependent dissipations, apparently because preferential reduction of high-frequency energy (by dissipation that increases with increasing frequency) is largely compensated by increased nonlinear energy transfers to high frequencies. In contrast to the insensitivity of predicted spectral levels, model predictions of skewness and asymmetry (statistical measures of the wave shapes) are sensitive to the frequency dependence of the dissipation. The observed spatial evolution of skewness and asymmetry is predicted qualitatively well by the model with frequency-dependent dissipation, but is predicted poorly with frequency-independent dissipation. Although the extension of the Boussinesq equations to breaking waves is ad hoc, a dissipation depending on the frequency squared (as previously suggested) reproduces well the observed evolution of wave frequency spectra, skewness, and asymmetry.

1. Introduction

The transformation of waves in the surf zone affects sediment transport, circulation, and other nearshore processes. However, no rigorous theory exists for the dynamically complex evolution of waves approaching and propagating across the surf zone. Models for the variation of total (frequency-integrated) energy [*Battjes and Janssen*, 1978; *Thornton and Guza*, 1983] do not predict wave spectra or wave shapes. Models based on the nonlinear shallow water equations with bore dissipation [*Wurjanto and Kobayashi*, 1991] predict accurately the evolution of sea surface elevation spectra both across the surf zone and in the run-up [*Kobayashi et al.*, 1989; *Cox et al.*, 1992, 1994; *Kobayashi and Wurjanto*, 1992; *Raubenheimer et al.*, 1995, 1996; *Raubenheimer and Guza*, 1996]. However, the long wave (i.e., nondispersive) approximation used in the shallow water equations restricts significantly the range of modeled frequencies. Additionally, unbroken waves are predicted to steepen and form shocks (bores) within a few wavelengths, so that the model must be initialized close to the surf zone. Models based on the nonlinear, dispersive, nondissipative Boussinesq equations predict accurately the evolution of broadband, nonbreaking waves observed in the laboratory and in the field [*Freilich and Guza*, 1984; *Elgar and Guza*, 1986; *Elgar et al.*, 1990]. Recently, empirical breaking-induced energy dissipation formulations have been included into both time domain [*Karambas and Koutitas*, 1992; *Schäffer et al.*, 1993, and references therein] and frequency domain Boussinesq models. Frequency domain models are considered here because time domain models require (usually unknown) downwave boundary conditions and are computationally intensive.

Empirical energy dissipation formulas have been incorporated into different nondissipative frequency domain models. *Liu* [1990] included a complex (equal real and imaginary parts) frequency-independent dissipation function [*Dally et al.*, 1985] in a parabolic Boussinesq model [*Liu et al.*, 1985] for the shoaling and breaking of cnoidal waves. Although wave heights were predicted correctly, the shapes of broken waves were modeled poorly. *Mase and Kirby* [1992] postulated a real, frequency(f)-dependent dissipation $d(f)E(f)$, where $d(f)$ consists of a constant term that drains en-

Paper number 97JC01565.
0148-0227/97/97JC-01565$09.00

ergy across all frequencies in proportion to the energy $E(f)$ at each frequency, and a term proportional to f^2 that increases the dissipation at high frequencies. Schematically, $d(f) = D(F + (1-F)f^2D')$, where the free parameter F controls the relative importance of the two terms, and D and D' are frequency-independent terms (related to the moments of the spectrum) that determine the total (frequency-integrated) dissipation. *Mase and Kirby* [1992] incorporated this dissipation into a hybrid Korteweg-de Vries (KdV) model, and *Kaihatu and Kirby* [1995] included the same $d(f)$ in nonlinear, parabolic, frequency domain mild-slope equations. In both cases, the models with $F = 0.5$ predict well the spectral evolution on a sloping laboratory beach for two different initial wave spectra. However, *Mase and Kirby* [1992] and *Kaihatu and Kirby* [1995] (hereinafter referred to collectively as MKK) remark that the generality of their dissipation formulation should be examined with additional observations.

When $F = 1$, the dissipation is linearly proportional to $E(f)$, a form referred to as frequency independent by *Eldeberky and Battjes* [1996], who incorporated this dissipation into extended Boussinesq equations [*Madsen and Sørensen*, 1993]. The predicted frequency spectra agreed with laboratory measurements.

In both MKK and *Eldeberky and Battjes* [1996] (hereinafter referred to as EB), the total energy dissipation in the nonlinear frequency domain models is constrained to equal that predicted by heuristic (but reasonably accurate) frequency-integrated models. The differences between the models used for the total energy (EB used *Battjes and Janssen* [1978], whereas MKK used *Thornton and Guza* [1983]) are of little consequence because free parameters in the models are selected to match the observed wave height decay (EB). Similarly, the choice of underlying nonlinear, frequency domain model (e.g., hybrid KdV equation, nonlinear mild-slope equations, or extended Boussinesq equations) is not critical because these models behave similarly in intermediate and shallow water depths. Given that the models for the total dissipation and nonlinear propagation are accurate, it is unclear why models with frequency-independent (EB) and frequency-dependent (MKK) dissipation both compare well with observations.

The purpose of this study is to assess frequency-dependent and frequency-independent dissipation forms by comparing model predictions to the same data sets. The 10 experimental cases include laboratory data used by MKK and EB, laboratory observations with bimodal frequency spectra [*Smith and Vincent*, 1992], and field data [*Elgar et al.*, 1997]. In addition to frequency spectra considered in past studies, the model-data comparisons include skewness and asymmetry (statistical measures of wave shapes).

A nonlinear Boussinesq model for the evolution of breaking waves is presented in section 2. The beach profiles and initial conditions for the cases studied are described in section 3, and optimal values for free model parameters are discussed in section 4. Observations and model predictions are compared in section 5, followed by a discussion and summary in sections 6 and 7, respectively.

2. Model

The evolution of waves approaching and propagating across a surf zone is modeled with the modified Boussinesq equations for normally incident nondissipative waves propagating over parallel depth contours [*Chen and Liu*, 1995]:

$$\zeta_t + [(\zeta+h)\Phi_{\alpha x}]_x + \left\{h\left[z_\alpha(h\Phi_{\alpha x})_x + \tfrac{1}{2}z_\alpha^2\Phi_{\alpha xx}\right]_x + \tfrac{1}{2}h^2[h\Phi_{\alpha x}]_{xx} - \tfrac{1}{6}h^3\Phi_{\alpha xxx}\right\}_x = 0, \quad (1)$$

$$\Phi_{\alpha t} + g\zeta + \tfrac{1}{2}(\Phi_{\alpha x})^2 + z_\alpha(h\Phi_{\alpha xt})_x + \tfrac{1}{2}z_\alpha^2\Phi_{\alpha xxt} = 0, \quad (2)$$

where $\Phi_\alpha(x,t)$ is the velocity potential at an arbitrary vertical elevation $z = z_\alpha(x)$, $\zeta(x,t)$ is the free surface displacement, $h(x)$ is the water depth, x is the cross-shore coordinate, and g is gravitational acceleration. The subscripts x and t denote spatial and temporal derivatives, respectively. With $z_\alpha = -0.522h$, equations (1) and (2) have approximately the same dispersive behavior as linear Stokes waves for water depths ranging from zero to half of the deep water wavelength [*Chen and Liu*, 1995]. This optimal water level is used here.

Substituting the Fourier representations for Φ_α and ζ

$$\Phi_\alpha(x,t) = \frac{1}{2}\sum_{n=1}^{N}\phi_n(x)e^{-in\omega t} + *, \quad (3)$$

$$\zeta(x,t) = \frac{1}{2}\sum_{n=1}^{N}\zeta_n(x)e^{-in\omega t} + *, \quad (4)$$

where ϕ_n and ζ_n are the Fourier coefficients of the velocity potential and free-surface displacement, respectively, ω is the frequency resolution, and the asterisk denotes complex conjugate, into (1) and (2) and eliminating ζ_n results in a set of fourth-order ordinary differential equations for ϕ_n. With slowly varying depth and negligible reflection, the equations reduce to a set of first-order ordinary differential equations,

$$\phi_{nx} = \left[ik_n - \frac{1}{2k_nW_n}(P_nk_{nx} + k_nR_nh_x)\right]\phi_n + \frac{\omega/2}{(\alpha+1/3)gh^3}\left[\sum_{s=1}^{n-1}\sigma_{ns}\phi_s\phi_{n-s} + \sum_{s=1}^{N-n}\gamma_{ns}\phi_s^*\phi_{n+s}\right], \quad (5)$$

where k_n (the wavenumber at frequency $n\omega$), W_n, P_n, R_n, σ_{ns}, and γ_{ns} in terms of h are given by *Chen and Liu* [1995] and $\alpha = -0.3855$. The terms in the square bracket in (5) correspond to linear dispersion and shoaling, and the summations over nonlinear terms represent cross-spectral mode coupling between near-resonantly interacting wave triads.

Given $\phi_n (n = 1, \cdots, N)$, the free surface displacement ζ_n is obtained from

$$g\zeta_n = in\omega\phi_n + in\omega\left[\alpha h^2 \phi_{nxx} + z_\alpha h_x \phi_{nx}\right] - \frac{1}{4}\left[\sum_{s=1}^{n-1} \phi_{sx}\phi_{(n-s)x} + 2\sum_{s=1}^{N-n} \phi_{sx}^* \phi_{(n+s)x}\right]. \quad (6)$$

The nondissipative model (5) is extended crudely into the surf zone by including breaking-induced energy dissipation. Following MKK, (5) is revised to

$$\phi_{nx} = \left[ik_n - \frac{1}{2k_n W_n}(P_n k_{nx} + k_n R_n h_x)\right]\phi_n - d_n\phi_n + \frac{\omega/2}{(\alpha + 1/3)gh^3}\left[\sum_{s=1}^{n-1} \sigma_{ns}\phi_s\phi_{n-s} + \sum_{s=1}^{N-n} \gamma_{ns}\phi_s^*\phi_{n+s}\right], \quad (7a)$$

where the damping coefficient of the nth Fourier component is given by

$$d_n = D\left[F + (1-F)G(f_n)\frac{\sum_{n=1}^{N}|a_n|^2}{\sum_{n=1}^{N} G(f_n)|a_n|^2}\right], \quad (7b)$$

with the dissipation function $D(x)$ and frequency-dependent function $G(f)$ specified below. The damping coefficient is much smaller than the wavenumber, and thus the nth Fourier coefficient of the free surface displacement in (7b) is approximated by its leading-order term a_n:

$$a_n = in\omega(1 - \alpha h^2 k_n^2)\phi_n / g. \quad (7c)$$

The dissipation function

$$D = \frac{3\sqrt{\pi}}{4h\sqrt{gh}} b \bar{f} H'_{\mathrm{rms}} \{1 + \tanh[8(H'_{\mathrm{rms}}/\gamma h - 1)]\} \times \left\{1 - \left[1 + (H'_{\mathrm{rms}}/\gamma h)^2\right]^{-5/2}\right\}, \quad (7d)$$

with

$$H'_{\mathrm{rms}} = 2\left(\sum_{n=1}^{N} |a_n|^2\right)^{1/2}, \quad (7e)$$

is chosen so that in shallow water the frequency-integrated dissipation derived from the linear version of (7a) (e.g., the nonlinear interaction terms are neglected) evolves as described by the frequency-integrated energy balance model of *Whitford* [1988]:

$$\frac{\mathrm{d}}{\mathrm{d}x}\left(\tfrac{1}{8}\rho g H_{\mathrm{rms}}^2 C_g\right) = \frac{3\sqrt{\pi}}{16h}\rho g b \bar{f} H_{\mathrm{rms}}^3 \{1 + \tanh[8(H_{\mathrm{rms}}/\gamma h - 1)]\} \times \left\{1 - \left[1 + (H_{\mathrm{rms}}/\gamma h)^2\right]^{-5/2}\right\}, \quad (8)$$

where C_g is the group velocity given by linear theory, ρ is the water density, $\bar{f}$ is the frequency corresponding to the centroid of the frequency spectrum, b and γ are adjustable constants, and H_{rms} is the root-mean-squared wave height. For the data considered here, H_{rms} predicted by the *Whitford* [1988] model were slightly more accurate than those predicted by the similar model of *Thornton and Guza* [1983] used by MKK. For cases in which both *Whitford* [1988] and *Thornton and Guza* [1983] models fit accurately the observed H_{rms}, predictions of the Boussinesq model (7a) are similar regardless of the model used to specify D in (7b).

The focus here is on the frequency dependence of the dissipation. The damping coefficient d_n (equation (7b)) has a frequency-independent part and a frequency-dependent part given by $G(f_n)$. In the following, unless otherwise noted, $G(f_n) = f_n^2$ as suggested by MKK. If $F = 1$, the damping coefficient d_n is independent of frequency and the Boussinesq model is equivalent to EB and will be called the *Eldeberky and Battjes* [1996] model (EBM). On the other hand, if F is not a priori equal unity (but is determined by fitting to the data), the model is called the *Mase and Kirby* [1992] and *Kaihatu and Kirby* [1995] model (MKKM).

For the data considered here, including an imaginary dissipation term with magnitude equal to the real part [*Liu*, 1990] did not alter significantly the predicted evolution of spectra, skewness, or asymmetry. Imaginary terms in d_n are equivalent to changes in the wavenumber k_n in (7a) and are expected to have a negligible effect if the imaginary part of $d_n \ll k_n$.

The model is initialized with Fourier coefficients of time series of sea surface elevation observed at the initial conditions [*Freilich and Guza*, 1984]. Results of numerical integration of (7) are used to calculate predicted spectra, significant wave heights (H_s based on the total variance of sea surface elevation over the modeled frequency band), and skewness and asymmetry at each shoreward measurement location.

3. Beach Profiles and Initial Conditions

The 10 experimental cases studied include run 1 in MKK, test 1c in the Delta Flume'93 experiment [*Arcilla et al.*, 1994] used by EB, cases 7, 8, and 9 of *Smith and Vincent* [1992], and five field data sets (09040400, 09041000, 09041600, 09060100, and 09221600) from the Duck 94 field experiment [*Elgar et al.*, 1997]. In both the MKK and *Smith and Vincent* [1992] experiments, the bathymetry consisted of a uniformly sloping bottom (solid lines in Figures 1b and 2c). The anomalous measurement at the shallowest gage location ($h = 0.025$ m) in run 1 [*Kirby and Kaihatu*, 1996] is not used in the model-data comparisons below. The data for test 1c were collected on a nearly full-scale, barred laboratory beach [*Eldeberky and Battjes*, 1996]. The water depth at Duck (solid line in Figure 3b) decreased gradually to a small sandbar in about 2-m depth ($x/\lambda_0 \approx 5.0$) and was nearly constant (less than 30 cm depth variation) between the sandbar and a steep (slope ≈ 0.1) beachface [*Elgar et al.*, 1997]. Changes in the beach profile were

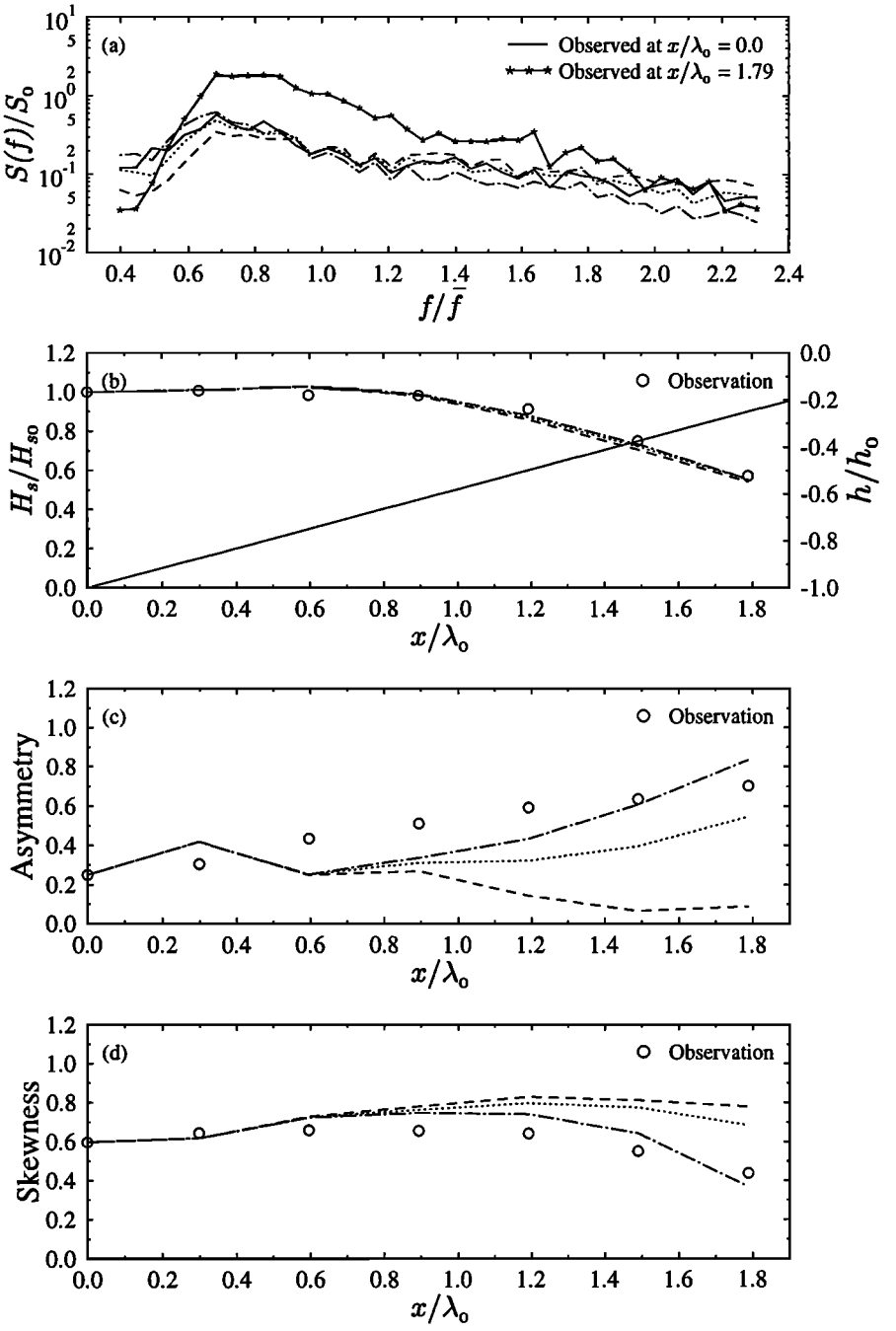

Figure 1. (a) Predicted and observed frequency spectra for run 1 at the normalized cross-shore location $x/\lambda_0 = 1.79$, where $\lambda_0 = 1.68$ m is the wavelength corresponding to the centroidal frequency of the initial ($x/\lambda_0 = 0$) spectrum; (b) corresponding normalized wave height H_s/H_{s0} (broken lines and open circles) and depth h/h_0 (solid line), where the initial significant wave height $H_{s0} = 0.07$ m and the initial depth $h_0 = 0.20$ m; (c) asymmetry; and (d) skewness versus normalized cross-shore coordinate. In each panel, the predictions are shown for $F = 0.0$ (dot-dashed line), $F = 1.0$ (dashed line), and the optimal F (dotted line, in this case $F = 0.4$).

small during the 18 days in September when the observations discussed here were obtained, but mean water depths (at any given cross-shore location) differed by as much as 125 cm between runs owing to tidal fluctuations.

For each case, the model is initialized at the deepest measurement location such that the water depth h_0 (given in Table 1) is less than half the deep water wavelength of the highest frequency considered. At the initial locations, $0.3 < (\bar{k}h_0)^2 < 0.7$, where $\bar{k}$ is the wavenumber at the centroidal frequency (Table 1), indicating that the energetic parts of the wave field are initially in shallow or intermediate water depth. Frequency spectra at the initial locations are unimodal

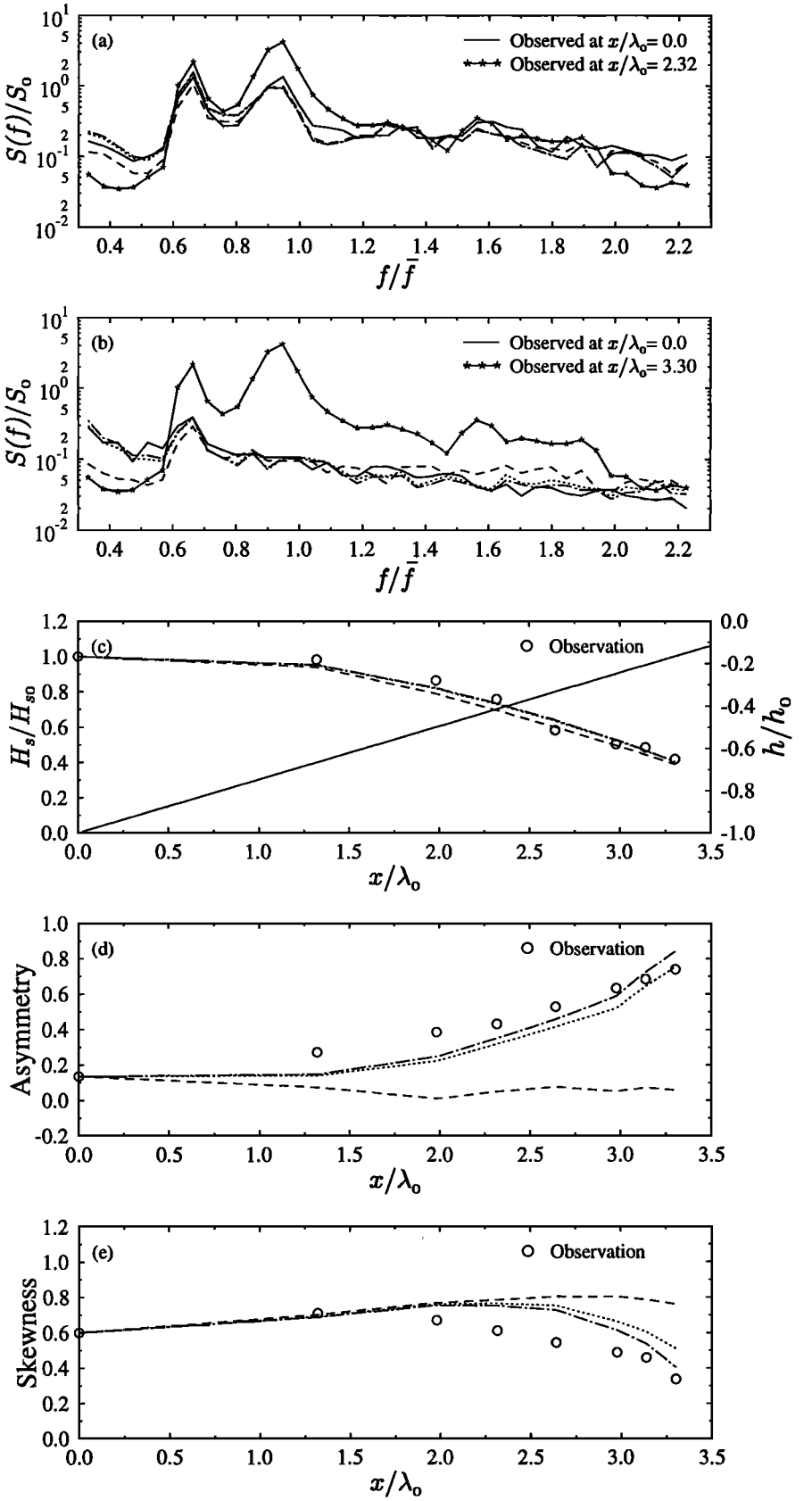

Figure 2. Predicted and observed frequency spectra for case 7 at the normalized cross-shore locations (a) $x/\lambda_0 = 2.32$ and (b) $x/\lambda_0 = 3.30$ with $\lambda_0 = 2.77$ m; (c) corresponding normalized wave height H_s/H_{s0} ($H_{s0} = 0.14$ m, broken lines and open circles) and depth h/h_0 ($h_0 = 0.37$ m, solid line); (d) asymmetry; and (e) skewness versus normalized cross-shore coordinate. In each panel, the predictions are shown for $F = 0.0$ (dot-dashed line), $F = 1.0$ (dashed line), and the optimal F (dotted line, in this case $F = 0.1$).

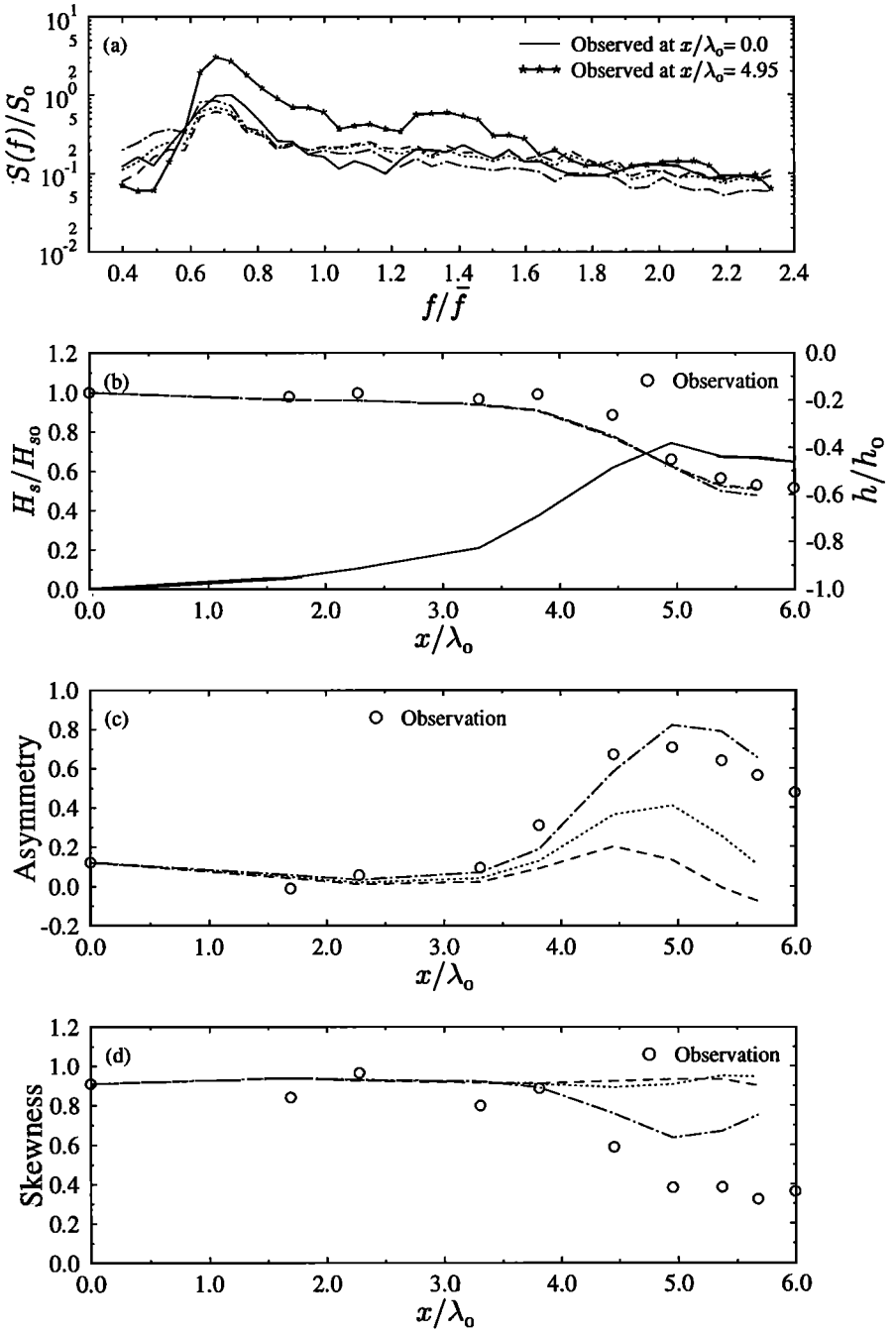

Figure 3. Same as figure 1, but for data set 09060100. The normalized cross-shore location in Figure 3a is $x/\lambda_0 = 4.95$ with $\lambda_0 = 48.43$ m. The initial significant wave height and depth in Figure 3b are $H_{s0} = 1.33$ m and $h_0 = 4.27$ m (the solid line in Figure 3b corresponds to the barred beach profile). The optimal $F = 0.6$.

and broad in laboratory run 1 (Figure 1a) and test 1c, and in the three Duck runs on September 4 (09040400, 09041000, and 09041600 collected 6 hours apart at different tidal stages). The selected *Smith and Vincent* [1992] spectra are strongly bimodal at the initial conditions, with comparable energy in the high-frequency "sea" peak and the low-frequency "swell" peak (Figure 2a). The moderately energetic wave fields (H_s is about 1.35 m at the initial conditions) in Duck runs 09060100 (Figure 3a) and 09221600 were dominated by narrowband swell.

4. Parameter Specification

Three free parameters (F, b, and γ) in the damped Boussinesq model (7) are not determined a priori or by initial conditions. First, values of b and γ were obtained by minimizing the normalized root-mean-squared error between measured and modeled (using equation (8)) total energy:

$$e_0 = \left\{ \frac{1}{M} \sum_n \frac{[E_{\text{meas}}(x_n) - E_{\text{model}}(x_n)]^2}{[E_{\text{meas}}(x_n)]^2} \right\}^{1/2}, \quad (9)$$

Table 1. Wave Parameters at the Initial Conditions

Case	H_s, m	f_p, Hz	$\bar{f}$, Hz	h_0, m	DOF	f_1-f_2, Hz	M	N
Run 1	0.07	0.6	0.768	0.20	60	0.3-1.8	6	148
Test 1c	0.56	0.122	0.149	4.06	54	0.06-0.4	11	82
Case 7	0.14	0.4/0.57	0.619	0.37	72	0.2-1.4	7	144
Case 8	0.14	0.4/0.57	0.594	0.37	72	0.2-1.4	7	144
Case 9	0.14	0.4/0.5	0.561	0.37	72	0.2-1.4	7	144
09040400	2.35	0.115	0.165	5.39	120	0.05-0.3	8	154
09041000	2.22	0.104	0.160	4.50	120	0.05-0.3	8	154
09041600	2.41	0.109	0.158	5.52	120	0.05-0.3	8	154
09060100	1.33	0.086	0.127	4.27	120	0.05-0.3	8	154
09221600	1.43	0.109	0.132	4.59	120	0.05-0.3	8	154

H_s is the significant wave height; f_p is the peak frequency; $\bar{f}$ is the centroid of the frequency spectrum; h_0 is the depth; DOF is the degrees of freedom; f_1-f_2 is the frequency band modeled; M is the number of measurement locations used for model-data comparisons; and N is the number of Fourier components in model computations.

where

$$E(x) = \tfrac{1}{8}\rho g H_{\mathrm{rms}}^2(x) = \rho g \int_{f_1}^{f_2} S(x,f)\mathrm{d}f, \qquad (10)$$

and $S(x,f)$ is the energy spectral density, f_1 and f_2 are low- and high-frequency cutoffs, respectively, and M is the number of comparison gages (Table 1). The error at each location is normalized with the total observed energy at that location, so that each measured energy is weighted equally in determining the optimal parameters. The optimal values of b (Table 2) are scattered over the interval 0.16–0.54. However, with $b = B^3$ and using the peak frequency (f_p) instead of the centroidal frequency ($\bar{f}$), $0.61 < B < 0.88$, which is close to the range given by *Whitford* [1988]. The optimal values of γ (Table 2) also fall into the expected range [*Lippmann et al.*, 1996]. Although the e_0 errors in fitting the total energy of bimodal cases (cases 7, 8, and 9 in Table 2) are usually larger than the unimodal cases, the errors in the total energy are all less than 10%. Neither observations nor model predictions near or on the steep shoreface at Duck are considered here because the measured total energy was not predicted accurately.

The total dissipation in the nonlinear Boussinesq model (equations (6) and (7)) is equal to the dissipation (with the same b and γ values) given by *Whitford* [1988] only when the nonlinear terms in the Boussinesq model are neglected. However, the differences are slight when nonlinearity is included, and observed significant wave heights are modeled accurately by the damped, nonlinear Boussinesq equations with b and γ values determined by optimal fits to the *Whitford* [1988] model (e.g., see Figures 1b, 2c, and 3b).

Table 2. Parameters Used in Model Predictions

	Bulk Model			MKKM			EBM	
Case	γ	b	e_0	F	e_1	e_2	e_1	e_2
Run 1	0.38	0.54	0.05	0.4	0.11	0.31	0.14	0.55
Test 1c	0.24	0.32	0.05	1.0	0.13	0.28	0.13	0.28
Case 7	0.38	0.31	0.09	0.1	0.12	0.24	0.16	0.71
Case 8	0.38	0.31	0.09	0.0	0.15	0.20	0.18	0.74
Case 9	0.40	0.33	0.10	0.0	0.16	0.28	0.18	0.80
09040400	0.34	0.16	0.05	1.0	0.14	0.56	0.14	0.56
09041000	0.34	0.24	0.10	0.9	0.12	0.65	0.13	0.68
09041600	0.34	0.18	0.03	1.0	0.12	0.57	0.12	0.57
09060100	0.30	0.38	0.06	0.6	0.13	0.63	0.13	0.75
09221600	0.30	0.42	0.08	1.0	0.13	0.65	0.13	0.65

The first two "bulk model" columns are γ and b values from fitting the *Whitford* [1988] model (equation (8)) to observed wave heights. The third column is the corresponding energy errors e_0 (equation (9)). Spectral errors e_1 (equation (11)) are given for models using optimal F values that minimize e_1 (MKKM [*Mase and Kirby*, 1992; *Kaihatu and Kirby*, 1995] columns) and using $F = 1.0$ (EBM [*Eldeberky and Battjes*, 1996] columns). The skewness and asymmetry errors e_2 (equation (12)) are based on the same values of b, γ, and F as the e_1 values.

After b and γ values are determined, optimal values of F in MKKM are calculated by minimizing spectral errors. To avoid weighting too heavily how well the spectral peak is modeled (which depends primarily on the fidelity of the *Whitford* [1988] model (8)) and to weigh more heavily discrepancies in model predictions at high frequencies, F was chosen by minimizing the root-mean-squared difference between the logarithms of measured and predicted spectra,

$$e_1 = \left\{ \frac{1}{M} \sum_n \frac{1}{f_2 - f_1} \int_{f_1}^{f_2} [\log S_{\text{meas}}(x_n, f) - \log S_{\text{model}}(x_n, f)]^2 \mathrm{d}f \right\}^{1/2}. \quad (11)$$

Optimal values of F and the corresponding values of e_1 are given in the columns labeled MKKM in Table 2.

5. Model-Data Comparisons

Predicted and observed spectra, significant wave heights, and skewness and asymmetry are shown in Figures 1–3 for three selected cases. Using optimal values of F (Table 2), the observed evolution of spectral shapes is modeled qualitatively well in these cases (compare solid with dotted lines in Figures 1a, 2a, 2b, and 3a). The evolution of a wave field with a bimodal frequency spectrum is modeled about as well as those with unimodal spectra (compare Figures 2a and 2b with Figures 1a and 3a), and the field data are modeled about as well as the laboratory data (compare Figure 3a with Figures 1a, 2a, and 2b). Note that the optimal $F = 0.4$ in run 1 (Table 2) is close to the $F = 0.5$ value used by MKK to model this same data set, and the optimal $F = 1.0$ in test 1c (Table 2) coincides with the value used by EB to model that data set. All 10 cases have similar e_1 errors ($0.11 < e_1 < 0.16$) using optimal F values (Table 2).

The optimal F values for the 10 cases span the entire possible range from 0.0 to 1.0 (Table 2). However, the model predictions are insensitive to the frequency dependence of the dissipation (i.e., the value of F). Model predictions using $F = 0.0$, $F = 1.0$, and the optimal F are similar (compare broken lines with each other in Figures 1a, 2a, 2b, and 3a). The values of the spectral error e_1 for frequency-independent ($F = 1.0$) dissipation are no more than one third larger than those for the optimal F (Table 2). The overall insensitivity of e_1

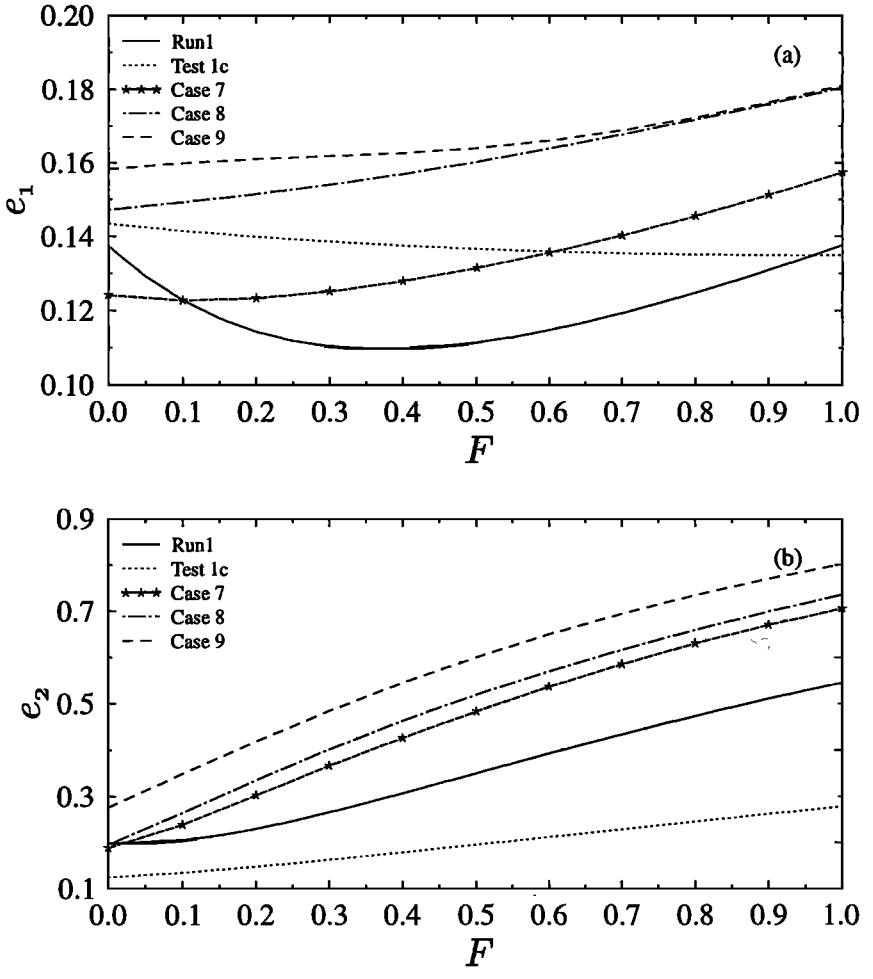

Figure 4. (a) Spectral error e_1 (see equation (11)), and (b) skewness and asymmetry error e_2 (see equation (12)) versus the dissipation weighting F (see equation (7b)) for five laboratory cases. Note the different vertical scales.

to variation of F for the five laboratory cases is shown in Figure 4a. Results for the field cases are similar (not shown). For all 10 cases, e_1 varies by less than 50% of its minimum value over the entire range.

In contrast to the insensitivity of predicted spectra to the frequency dependence of the dissipation, model predictions of skewness and asymmetry are sensitive to F (Figures 1c, 1d, 2d, 2e, 3c, and 3d). Skewness is the deviation of the fluctuating sea surface from symmetry about a horizontal plane and is nonzero for waves with sharp crests and broad, flat troughs. Asymmetry is related to deviations from symmetry about a vertical plane, as occurs if waves are pitched forward [*Masuda and Kuo*, 1981; *Elgar and Guza*, 1985]. The skewness and asymmetry of a linear Gaussian wave field are zero, and the nonzero values of the skewness and asymmetry characterize the nonsinusoidal shapes of nonlinear waves in the sure zone. Errors in the predicted skewness and asymmetry are defined here as

$$e_2 = \left\{ \frac{1}{M} \sum_n \left([a_{\text{meas}}(x_n) - a_{\text{model}}(x_n)]^2 + [s_{\text{meas}}(x_n) - s_{\text{model}}(x_n)]^2 \right) \times \left([a_{\text{meas}}(x_n)]^2 + [s_{\text{meas}}(x_n)]^2 \right)^{-1} \right\}^{1/2}, \quad (12)$$

where a is the asymmetry and s is the skewness. For all the laboratory cases (Figure 4b) and field cases (not shown), e_2 monotonically increases with increasing F. Furthermore, the increase of e_2 as F increases from 0.0 to 1.0 is significant (Figure 4b shows e_2 increases by at least a factor of 2 as F increases from 0.0 to 1.0 for the laboratory cases). For both laboratory and field cases, skewness and asymmetry are predicted best with $F = 0$, corresponding to the strongest frequency dependence of dissipation, and predicted poorly with $F = 1$, corresponding to frequency-independent dissipation (Figure 5).

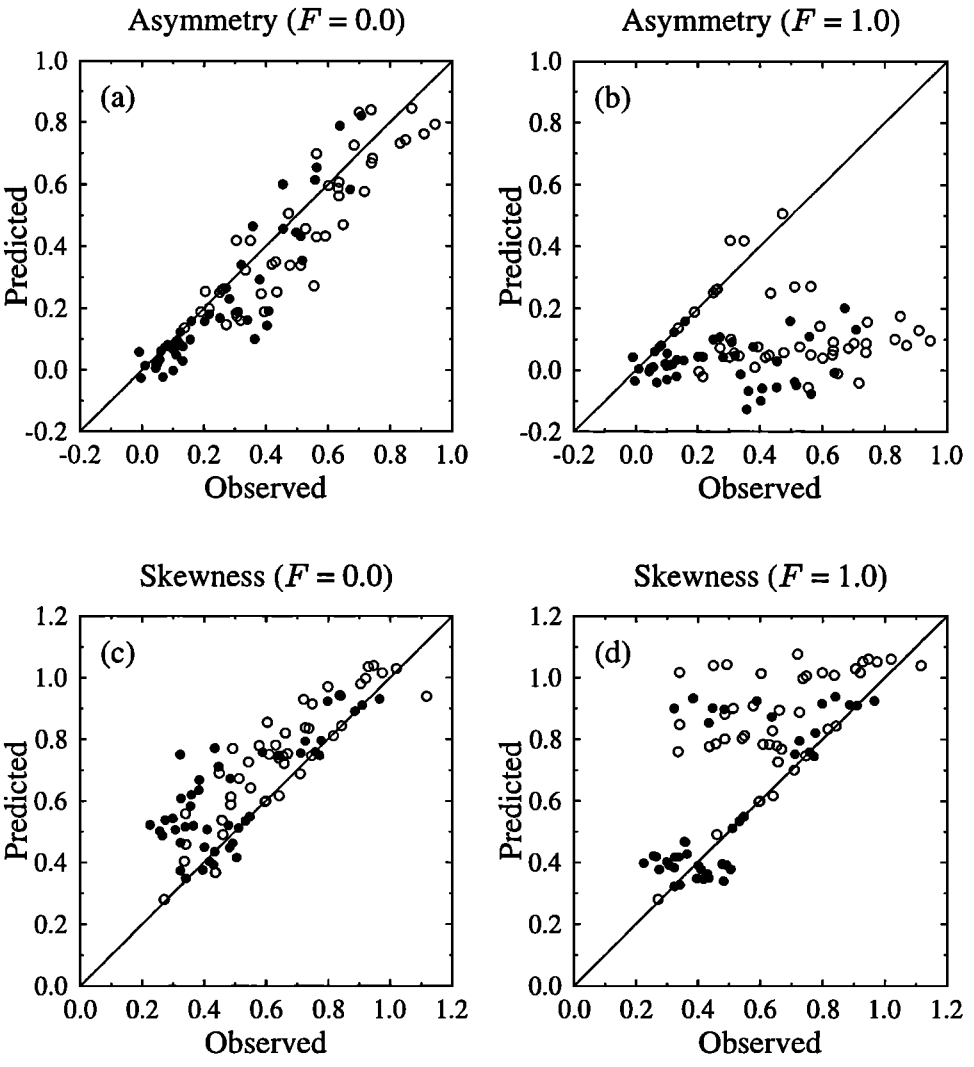

Figure 5. Comparison between observed and predicted (top) asymmetry and (bottom) skewness with (left) $F = 0.0$ and (right) $F = 1.0$ for 10 studied cases. Open and solid circles represent laboratory and field data, respectively.

Using an F value smaller than the (usually nonzero) F that is optimal for spectral prediction improves significantly predictions of skewness and asymmetry with little deterioration in predictions of spectra (Figures 1–3). Unless spectral errors are weighted heavily compared to skewness and asymmetry errors, $F = 0.0$ provides the best overall fit.

6. Discussion

The predicted spectra are not only insensitive to the value of F, but are also insensitive to the precise functional form of the dissipation. Figures 1–3 are based on a quadratic frequency dependence (i.e., $G(f_n) = f_n^2$ in (7b)), but the spectral predictions are similar for $G(f_n) = f_n^4$, f_n^2, or f_n. For example, minimum values of e_1 for f^4-dependent dissipation are close to those for f^2-dependent dissipation, and the dependence on F for f^4-dependent dissipation remains weak for most of the data sets. Errors in skewness and asymmetry predictions using $G(f_n) = f_n^4$ are similar to those using $G(f_n) = f_n^2$ (Figure 4b and Figure 5).

When the nonlinear terms in the Boussinesq equations are suppressed, and all other initial conditions and total dissipation parameters (i.e., γ and b) are the same as used in the calculations with nonlinearity included, predicted high-frequency spectral levels are dramatically reduced with decreasing F (Figure 6). The contrast between $G(f_n) = f_n^2$ model results with (Figure 3a) and without (Figure 6) nonlinearity suggests that nonlinear energy transfers compensate approximately for enhanced dissipation at high frequencies when F is small, resulting in insensitivity of predicted high-frequency spectral levels to the value of F. Consistent with the suggested importance of nonlinear, cross-spectral energy transfers in maintaining energy levels at high frequency, additional simulations (not shown) indicate that nonlinear energy transfers rapidly restore high-frequency energy levels to approximately their original nonzero values even when artificially reduced to nearly zero in the initial conditions.

During propagation across the surf zone, the spectral levels in the high-frequency peak of an initial bimodal spectra decrease such that at the shallowest gage only the low-frequency swell peak remains (e.g., Figure 2b). *Smith and Vincent* [1992] suggested that the preferential decay of the sea peak could be caused by a bottom friction that increases with increasing frequency, by an enhancement of breaking at sea frequencies owing to low-frequency orbital velocities, or by resonant interactions that transfer energy from the sea peak to high frequencies where it is rapidly dissipated. Model results (Figure 7) [see also *Elgar and Guza*, 1986] demonstrate that nonlinear interactions alone can explain qualitatively the preferential decay of a sea peak. The model was initialized in the same water depth and with the same Fourier coefficients as for the model-data comparisons (Figure 2), but shoaling and dissipation in the subsequent propagation were suppressed by holding the depth constant and setting dissipation terms equal to zero. Nonlinear interactions alone cause a significant decay of the sea peak, transferring energy into both the spectral valley between the swell and sea peaks and into frequencies lower than the swell peak. The longer distances required for the sea peak to decay in constant depth (Figure 7) relative to those on a sloping bottom (Figure 2) are expected because the decreasing depth accelerates the nonlinear energy transfers.

Dissipation is cumulatively the dominant term in spectral evolution across the surf zone. However, local changes in spectral levels resulting from nonlinear interactions can exceed dissipation rates [*Elgar et al.*, 1997], and the interactions between near-resonant energy transfers and dissipation are complex. Nonlinear energy transfers appear both to maintain energy levels when dissipation is enhanced at high frequencies by breaking and to drain energy preferentially from the high-frequency peak of a bimodal spectrum.

7. Summary

The frequency dependence of wave-breaking induced dissipation is investigated by comparing predictions of

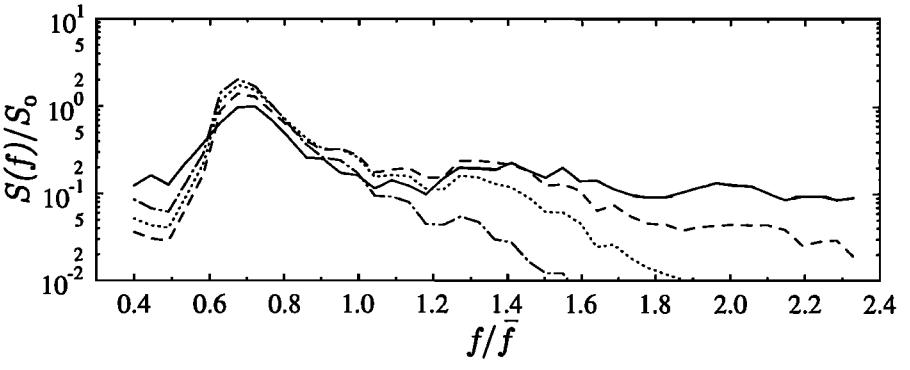

Figure 6. Predicted and observed normalized frequency spectra for data set 09060100 at normalized cross-shore location $x/\lambda_0 = 4.95$. Observations (solid line) and model predictions for $F = 0.0$ (dot-dashed line), $F = 1.0$ (dashed line), and optimal $F = 0.6$ (dotted line) are shown. The nonlinear terms in the model have been suppressed, resulting in underprediction of high-frequency spectral levels.

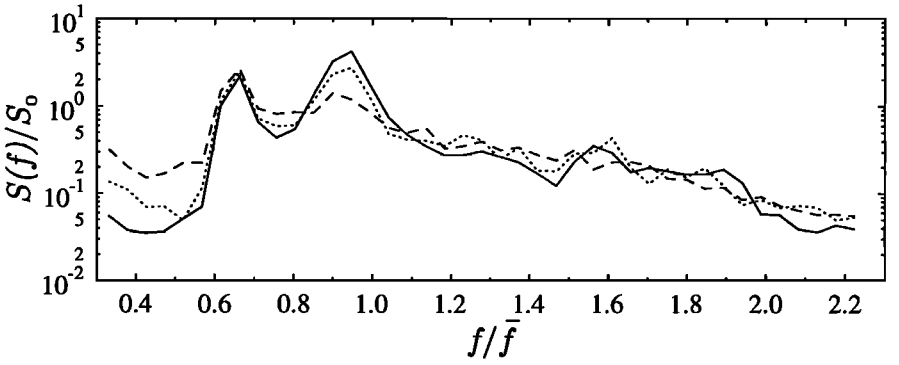

Figure 7. Predicted normalized frequency spectra for case 7 at normalized cross-shore locations x/λ_0 equal to 0.0 (solid line), 3.25 (dotted line), and 7.58 (dashed line). The depth is held equal to the depth at the initial location, and dissipation in the model is suppressed. Nonlinear terms reduce the energy levels of the high-frequency "sea peak" ($f/\bar{f} \approx 0.92$).

shallow water wave propagation models based on Boussinesq equations with field and laboratory observations. The range of modeled frequencies is roughly $0.3\bar{f}$–$2.5\bar{f}$, where $\bar{f}$ is the centroidal frequency at the location where the model is initialized. The total (frequency-integrated) breaking-wave dissipation in the Boussinesq model is a priori constrained to yield approximately the result of *Whitford* [1988], with the free parameters selected to optimize the fit to the observed total energy for each experimental case. Observed spectra are compared with those predicted by the Boussinesq model with frequency-independent dissipation that depends only on the energy levels at each frequency [after *Eldeberky and Battjes*, 1996], and with a dissipation that is weighted toward high frequency through an f^2 frequency dependence [after *Mase and Kirby*, 1992; *Kaihatu and Kirby*, 1995]. The different dissipation models have not been compared previously with the same data sets. For the 10 cases investigated in this study, the model-data agreement is similar and qualitatively good for both frequency-independent and f^2 frequency-dependent dissipation. Similar spectral evolution is also predicted for an f^4 dissipation. The predicted spectral levels at high frequencies (e.g., above the spectral peak) are insensitive to the frequency dependence of the dissipation because increased dissipation at high frequencies is compensated approximately by increased nonlinear energy transfers. In contrast to the insensitivity of predicted spectra, model predictions of skewness and asymmetry (statistical measures of wave shapes) are sensitive to the frequency dependence of the dissipation. Frequency-independent dissipation yields poor wave shape predictions, whereas frequency-dependent dissipation reproduces the observed spatial evolution of skewness and asymmetry. Although the extension of the Boussinesq equations to breaking waves is ad hoc, a dissipation depending on f^2 (similar to that suggested by *Mase and Kirby* [1992]) reproduces well the observed evolution of wave frequency spectra, skewness, and asymmetry.

Acknowledgments. This research was supported by a Mellon Foundation grant to the Center for Coastal Studies, the Office of Naval Research (Coastal Dynamics), and the National Science Foundation (CoOP program). We thank J.T. Kirby, A.S. Arcilla, Y. Eldeberky, C.L. Vincent, and J. Smith for generously providing their experimental data. J.T. Kirby, Wendell Brown, and an anonymous reviewer made helpful suggestions.

References

Arcilla, A. S., J. A. Roelvink, B.A. O'Connor, A. Reniers, and J.A. Jimenez, The Delta Flume'93 experiment, in *Coastal Dynamics'94*, pp. 488–502, Am. Soc. of Civ. Eng., New York, 1994.

Battjes, J. A., and J. P. F. M. Janssen, Energy loss and set-up due to breaking of random waves, in *Proceedings of the 16th International Conference on Coastal Engineering*, pp. 569–587, Am. Soc. of Civ. Eng., New York, 1978.

Chen, Y., and P. L.-F. Liu, Modified Boussinesq equations and associated parabolic models for water wave propagation, *J. Fluid Mech.*, *288*, 351–381, 1995.

Cox, D. T., N. Kobayashi, and A. Wurjanto, Irregular wave transformation processes in surf and swash zones, in *Proceedings of the 23th International Conference on Coastal Engineering*, pp. 156–169, Am. Soc. of Civ. Eng., New York, 1992.

Cox, D. T., N. Kobayashi, and D. L. Kriebel, Numerical model verification using SUPERTANK data in surf and swash zones, in *Coastal Dynamics'94*, pp. 248-262, Am. Soc. of Civ. Eng., New York, 1994.

Dally, W. R., R. G. Dean, and R. A. Dalrymple, Wave height variation across beaches of arbitrary profile, *J. Geophys. Res.*, *90*, 11,917–11,927, 1985.

Eldeberky, Y., and J. A. Battjes, Spectral modeling of wave breaking: Application to Boussinesq equations, *J. Geophys. Res.*, *101*, 1253–1264, 1996.

Elgar, S., and R. T. Guza, Observations of bispectra of shoaling surface gravity waves, *J. Fluid Mech.*, *161*, 425–448, 1985.

Elgar, S., and R. T. Guza, Nonlinear model predictions of bispectra of shoaling surface gravity waves, *J. Fluid Mech.*, *167*, 1–18, 1986.

Elgar, S., M. H. Freilich, and R. T. Guza, Model-data comparisons of moments of nonbreaking shoaling surface gravity waves, *J. Geophys. Res.*, *95*, 16,055–16,063, 1990.

Elgar, S., R. T. Guza, B. Raubenheimer, T. H. C. Herbers, and E. L. Gallagher, Spectral evolution of shoaling and

breaking waves on a barred beach, *J. Geophys. Res., 102,* 15,797–15,805, 1997.

Freilich, M. H., and R. T. Guza, Nonlinear effects on shoaling surface gravity waves, *Philos. Trans. R. Soc. London A, 311,* 1–41, 1984.

Kaihatu, J. M., and J. T. Kirby, Nonlinear transformation of waves in finite water depth, *Phys. Fluids, 7,* 1903–1914, 1995.

Karambas, T. V., and C. Koutitas, A breaking wave propagation model based on the Boussinesq equations, *Coastal Eng., 18,* 1–19, 1992.

Kirby, J. T., and J. M. Kaihatu, Structure of frequency domain models for random wave breaking, in *Proceedings of the 25th International Conference on Coastal Engineering,* pp. 1144–1155, Am. Soc. of Civ. Eng., New York, 1996.

Kobayashi, N., and A. Wurjanto, Irregular wave setup and run-up on beaches, *J. Waterway Port Coastal and Ocean Eng., ASCE, 118,* 368–386, 1992.

Kobayashi, N., G. S. DeSilva, and K. D. Watson, Wave transformation and swash oscillation on gentle and steep slopes, *J. Geophys. Res., 94,* 951–966, 1989.

Lippmann, T. C., A. H. Brookins, and E. B. Thornton, Wave energy transformation on natural profiles, *Coastal Eng., 27,* 1–20, 1996.

Liu, P. L.-F., Wave transformation, in *The Sea: Ocean Engineering Science,* edited by Le Méhauté and D. M. Hanes, vol. 9(A), pp. 27–63, John Wiley, New York, 1990.

Liu, P. L.-F., S. B. Yoon, and J. T. Kirby, Nonlinear refraction-diffraction of waves in shallow water, *J. Fluid Mech., 153,* 185–201, 1985.

Madsen, P. A., and O. R. Sørensen, Bound waves and triad interactions in shallow water, *Ocean Eng., 20,* 359–388, 1993.

Mase, H., and J. T. Kirby, Hybrid frequency-domain KdV equation for random wave transformation, in *Proceedings of the 23rd International Conference on Coastal Engineering,* pp. 474–487, Am. Soc. of Civ. Eng., New York, 1992.

Masuda, A., and Y. Y. Kuo, Bispectra for the surface displacement of random gravity waves in deep water, *Deep Sea Res., 28,* 223–237, 1981.

Raubenheimer, B., and R. T. Guza, Observations and predictions of runup, *J. Geophys. Res., 101,* 25,575–25,587, 1996.

Raubenheimer, B., R. T. Guza, S. Elgar, and N. Kobayashi, Swash on a gently sloping beach, *J. Geophys. Res., 100,* 8751–8760, 1995.

Raubenheimer, B., R. T. Guza, and S. Elgar, Wave transformation across the inner surf zone, *J. Geophys. Res., 101,* 25,589–25,597, 1996.

Schäffer, H. A., P. A. Madsen, and R. Deigaard, A Boussinesq model for waves breaking in shallow water, *Coastal Eng., 20,* 185–202, 1993.

Smith, J. M., and C. L. Vincent, Shoaling and decay of two wave trains on beach, *J. Waterway Port Coastal Ocean Eng., ASCE, 118,* 517–533, 1992.

Thornton, E. B., and R. T. Guza, Transformation of wave height distribution, *J. Geophys. Res., 88,* 5925–5938, 1983.

Whitford, D. J., Wind and wave forcing of longshore currents across a barred beach, Ph.D. thesis, Naval Postgrad. School, Monterey, Calif., 1988.

Wurjanto, A., and N. Kobayashi, Numerical model for random waves on impermeable coastal structures and beaches, *Res. Rep. CACR-91-05,* Cent. for Appl. Coastal Res., Univ. of Del., Newark, 1991.

Y. Chen and R.T. Guza, Center for Coastal Studies, Scripps Institution of Oceanography, La Jolla, CA 92093-0209. (e-mail: yongze@coast.ucsd.edu; rtg@coast.ucsd.edu)

S. Elgar, School of Electrical Engineering and Computer Science, Washington State University, Pullman, WA 99164-2752. (e-mail: elgar@eecs.wsu.edu)

(Received July 26, 1996; revised April 1, 1997; accepted May 7, 1997.)